ELSEVIER

Contents lists available at ScienceDirect

# Water Research

journal homepage: www.elsevier.com/locate/watres



# A mechanistic surface complexation model for glyphosate adsorption to ferrihydrite in competition with phosphate

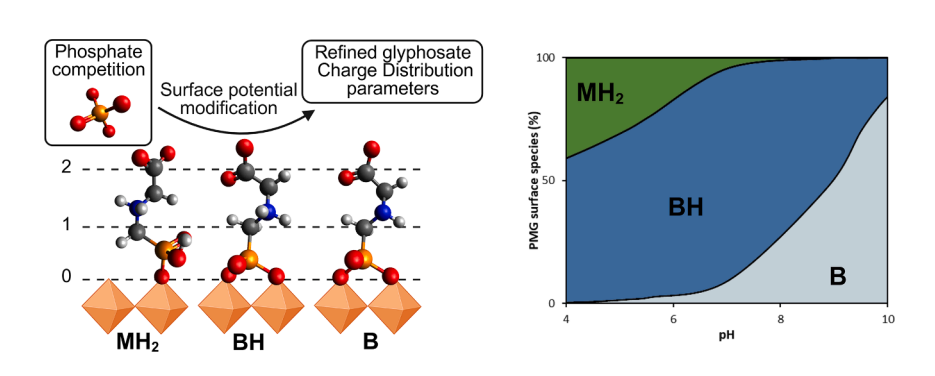
Bram Geysels a,b,\* D, Tjisse Hiemstra D, Arnoldus W.P. Vermeer D, Jan E. Groenenberg

- <sup>a</sup> Soil Chemistry Group, Wageningen University & Research, P.O. BOX 47, Wageningen 6700 AA, the Netherlands
- <sup>b</sup> INVITE GmbH, Otto-Bayer-Straße 32 D-51061 Cologne, Germany
- <sup>c</sup> Formulation Technology, 2022 ES Deutschland GmbH (ENVU), Alfred Nobel Str. 50 40789 Monheim am Rhein, Germany

#### HIGHLIGHTS

- Glyphosate sorption experiments on ferrihydrite in wide concentration- and pH range.
- Competitive adsorption with phosphate for surface potential modification.
- Consistent, mechanistic, quantitative model of glyphosate sorption to ferrihydrite.

#### G R A P H I C A L A B S T R A C T



#### ARTICLE INFO

Keywords:
Pesticide
Metal (hydr)oxides
Nanoparticles
Charge distribution
MO/DFT
Surface speciation

## ABSTRACT

The adsorption and mobility of glyphosate (PMG) in soils, sediments, natural waters, and wastewater treatment sludge are controlled by small-sized metal (hydr)oxides and affected by competition with phosphate. In this study, the adsorption of PMG to ferrihydrite, a ubiquitous nano-sized iron (hydr)oxide, is measured by batch adsorption experiments at a wide concentration ( $\sim$ 0.02 – 0.6 mM) and pH range ( $\sim$ 4–10), in the absence and presence of phosphate. The adsorption data were interpreted using the charge distribution and multisite ion complexation (CD-MUSIC) model for ferrihydrite. Including phosphate as a competitor induces electrostatic changes on the surface potential, independently of glyphosate adsorption, which allowed us to accurately distinguish between the chemical affinity and electrostatic effects contributing to PMG adsorption to ferrihydrite. PMG binds primarily as a binuclear bidentate complex, of which the amino group may protonate (log $K_{\rm H}$ =7.9). Only at low pH and high PMG surface loading, when binuclear bidentate binding sites become scarce, a monodentate complex with protonated amino and phosphonate groups becomes prominent. Phosphate effectively electrosase PMG adsorption and contributes to its enhanced mobility. The resulting CD model provides a quantitative and mechanistic description of PMG adsorption to ferrihydrite, which can be used for improved predictions of the environmental fate of PMG and its water removal effectiveness.

E-mail address: bram.geysels@wur.nl (B. Geysels).

<sup>\*</sup> Corresponding author.

#### 1. Introduction

Glyphosate (N-phosphonomethyl glycine, PMG) is a chemically atypical pesticide due to its high polarity and multiple ionizable functional groups. Its adsorption to surfaces is consequently a complex process with multiple possible surface species, which all have multiple protonation states (Borggaard and Gimsing, 2008; Sprankle et al., 1975). Due to its size and flexibility, adsorbed glyphosate surface complexes can allocate their charges to multiple positions in the interface and correspondingly alter the electrostatic potential (Geysels et al., 2025b).

The phosphonate group of PMG is highly reactive to natural metal (hydr)oxides (Barja and Dos Santos Afonso, 2005; Sheals et al., 2002; Waiman et al., 2012), determining the adsorption of PMG and its environmental mobility (Borggaard and Gimsing, 2008; Ololade et al., 2014). Despite its supposed immobility in soils, PMG contamination of surface and groundwater is widespread (Carretta et al., 2022; Peruzzo et al., 2008; Zhang et al., 2024). Recent findings further show urban use as a major source of PMG pollution of natural waters (Schwientek et al., 2024), and conventional wastewater treatment plants appear to be ineffective in sufficiently removing of PMG (Botta et al., 2009; Hanke et al., 2010; Schwientek et al., 2024; Venditti et al., 2023). In these conventional plants, the main mechanism for PMG removal is via adsorption to iron minerals in the activated sludge, which are formed from iron salt additions (Poiger et al., 2020; Venditti et al., 2023).

Most research about the interaction of PMG with metal (hydr)oxides has focused on goethite ( $\alpha$ -FeOOH) as it is the most ubiquitous crystalline iron (hydr)oxide (Barja and Dos Santos Afonso, 2005; Dideriksen and Stipp, 2003; Geysels et al., 2025b; Jonsson et al., 2008; Sheals et al., 2003, 2002; Waiman et al., 2016, 2013, 2012). However, in natural systems, poorly crystalline and nano-scale metal (hydr)oxides are often more important in determining the reactivity due to their high specific surface area (SSA) (Mendez et al., 2022, 2020).

The most prevalent non-crystalline iron (hydr)oxide in the environment is ferrihydrite (Guo and Barnard, 2013). It is unstable in isolation as a precursor to crystalline iron (hydr)oxides, such as goethite, lepidocrocite, and hematite, but is stabilized in the presence of phosphate (PO<sub>4</sub>) and natural organic matter (NOM) (Jambor and Dutrizac, 1998). This nano oxide material is considered to be a better proxy for the ion metal (hydr)oxide interaction in soils and sediments than goethite (Mendez et al., 2022, 2020). As a precursor to more crystalline iron (hydr)oxides, ferrihydrite is an important and highly reactive iron mineral formed after addition of iron salts in waste water treatment plants (Zhang et al., 2019), and the dominant iron mineral in groundwater treatment plants (Likus et al., 2021; Qu et al., 2019).

Nano-sized ferrihydrite has distinct adsorptive properties. For example, phosphate surface complexes show an enhanced protonation on ferrihydrite that is not observed for crystalline goethite (Hiemstra and Zhao, 2016). In addition, the crystal structure of ferrihydrite consists of a considerable amount of surface sites that can accommodate mononuclear bidentate complexation (Hiemstra, 2013), while on well-crystalized goethite, these sites are limited (Livi et al., 2023).

The number of studies about the PMG binding to ferrihydrite is limited (Gimsing and Borggaard, 2007; Li and Jaisi, 2019; Li et al., 2023; Pereira et al., 2019), and they lack a mechanistic description of the adsorption behavior. Furthermore, no attempts were made to scale the adsorption to the surface area, which is highly variable for poorly crystalline ferrihydrite (Mendez and Hiemstra, 2020a). In two of these works, the PMG adsorption to ferrihydrite was studied by attenuated total reflectance Fourier transformed infrared (ATR-FTIR) spectroscopy (Li et al., 2023; Pereira et al., 2019). The binding mode and protonation of the surface complexes remain speculative in the PMG surface speciation, while they are essential factors governing the pH and concentration dependency of the adsorption process.

While PMG binding to metal (hydr)oxides is strong in synthetic monocomponent systems, it may be different in natural systems due to the presence of important competitors that impact the partitioning of PMG. The two main competitors to metal (hydr)oxide sorption in the environment are NOM and  $PO_4$ ; for goethite, both have been observed to decrease PMG adsorption considerably (Arroyave et al., 2017, 2016; Day et al., 1997; Dideriksen and Stipp, 2003; Geysels et al., 2025a; Waiman et al., 2016).

The interaction of PMG and  $PO_4$  is of particular concern as PMG is heavily applied in conventional agriculture, often coinciding with high  $PO_4$  fertilizer inputs that may decrease the PMG adsorption in soils (De Gerónimo and Aparicio, 2022; De Jonge et al., 2001; Laitinen et al., 2008; Munira et al., 2016). At the same time, as PMG can eventually degrade to  $PO_4$  (Sprankle et al., 1975; Sun et al., 2019). PMG application increases the phosphorus (P) status in soils (Hébert et al., 2019). This mutual interaction shows that competition with  $PO_4$  is essential to accurately assess the mobility of PMG in soils. Wastewater also contains high levels of  $PO_4$ , as it is the primary reason for the iron salt addition to wastewater treatment sludge, and its competition to adsorption might contribute to the incomplete removal of PMG.

Surface complexation modeling (SCM) can be a valuable tool in describing, understanding, and predicting the adsorption of ions on metal (hydr)oxides. When rooted in a solid mechanistic background, it can describe and reliably predict the competition between different ionic species. Information about the surface speciation at the microscopic scale is then of great value, particularly in relation to the denticity and protonation state of surface complexes, as these important factors determine the interfacial distribution of charge and the corresponding electrostatic effects, controlling the pH and loading dependency of the adsorption and especially competition with other ions.

In the present study, we will use the charge distribution (CD) model as it has been successful in describing the adsorption of many oxyanions (PO<sub>4</sub>, AsO<sub>4</sub>, As(OH)<sub>3</sub>, CO<sub>3</sub>, Si(OH)<sub>4</sub>, B(OH)<sub>3</sub>; Hiemstra, 2018; Hiemstra and Zhao, 2016; Van Eynde et al., 2020) and metal cations (alkali earth ions, Zn, Cu; Mendez and Hiemstra, 2020b; Van Eynde et al., 2022) to ferrihydrite, as well as its competitive and cooperative interaction.

To improve our insights into the adsorption of PMG and its competition with oxyanions, we will study the binding of PMG to ferrihydrite as a function of pH, surface loading, and different levels of PO<sub>4</sub>. With this, we will develop a model that describes the PMG surface speciation and corresponding interfacial electrostatic effects in a wide range of environmental conditions. The model development will be constrained by calculating the interfacial surface charge distribution by molecular orbital (MO) density functional theory (DFT) geometry optimization. These simulations will additionally be used to calculate theoretical infrared spectra of the surface species, which will be used to analyze literature spectroscopy data. The findings of each aspect of the PMG sorption process to ferrihydrite will be discussed, and in each section will be compared to PMG complexation to goethite (Geysels et al., 2025b). Combined, we provide a quantitative, mechanistic understanding of PMG binding to ferrihydrite, which will contribute to improved prediction of the availability, mobility, and transport of PMG in the environment.

#### 2. Materials & methods

## 2.1. Ferrihydrite synthesis

Ferrihydrite was prepared as described by Mendez and Hiemstra (2020a). In short, 3.7 mM of Fe(NO<sub>3</sub>)<sub>3</sub> was dissolved in 10 mM HNO<sub>3</sub> and neutralized stepwise with 20 mM NaOH until a pH of >6.0 was reached. This suspension was centrifuged for 45 min at 3500 g, followed by the removal of the supernatant and resuspension of the particles in 10 mM NaNO<sub>3</sub> to obtain a final concentration of  $\sim\!2$  g ferrihydrite  $l^{-1}$ . The suspension was stirred for 24 h (final aging time) and purged with N<sub>2</sub> continuously to avoid the inference of atmospheric CO<sub>2</sub>.

Two ferrihydrite stocks were prepared for the monocomponent PMG and the PO<sub>4</sub> competition adsorption experiments, respectively. From each stock, a sample of the ferrihydrite suspension was taken and

B. Geysels et al. Water Research 288 (2026) 124634

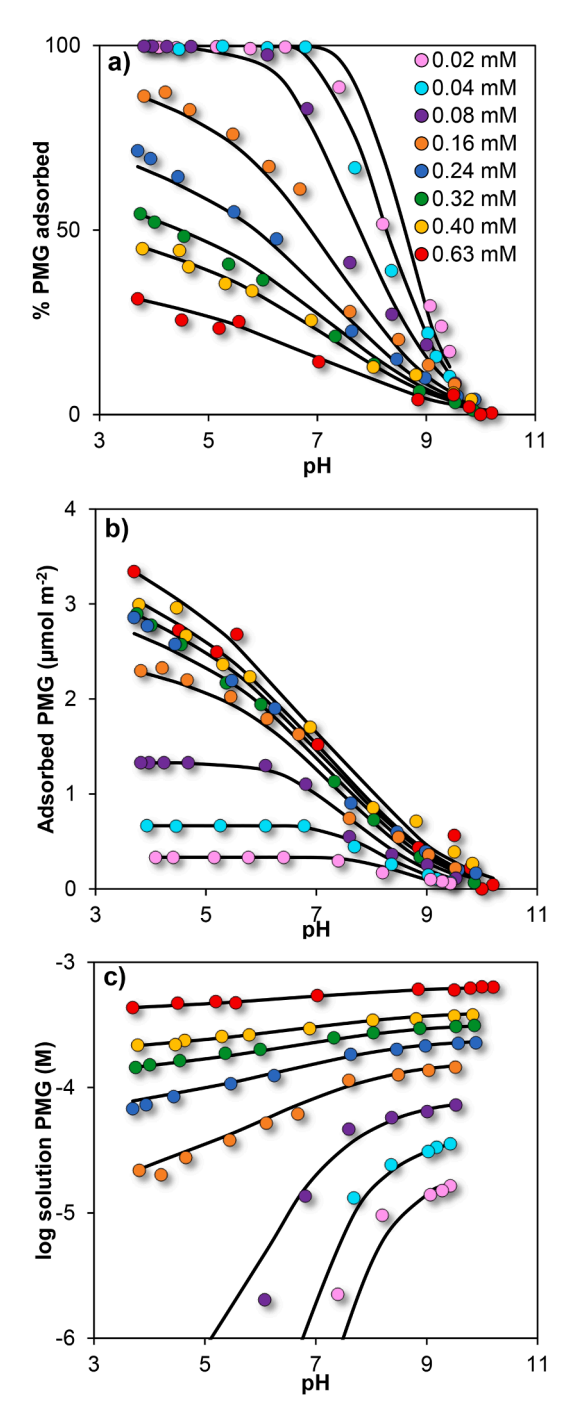


**Fig. 1.** Percentage adsorbed PMG (a), PMG surface loading (b), and logarithm of the equilibrium concentration in solution (c) as a function of pH in monocomponent PMG-ferrihydrite systems of 96 mg  $\rm L^{-1}$  ferrihydrite (618 m² g $^{-1}$ ) with 0.01 M NaNO3 as a background. Solid lines represent the model predictions using the parameters determined in this study (Table 1). Data points with excessive Fe concentration are not shown in (c) (see text).

dissolved in 0.8 M  $\rm H_2SO_4$  to measure the total iron (Fe) content with inductively coupled plasma optical emission spectroscopy (ICP-OES).

The specific surface area (SSA) of our ferrihydrite was determined by using  $PO_4$  as a probe ion, as described before, since more traditional gas adsorption techniques require the drying of the products, which leads to irreversible aggregation of the individual ferrihydrite particles (Hiemstra et al., 2019; Mendez and Hiemstra, 2020a). Briefly,  $PO_4$  adsorption experiments are carried out at 4 varying pH values parallel to the PMG adsorption experiments with the used ferrihydrite stock. The

SSA is fitted as a single free parameter in the CD model for ferrihydrite to evaluate these using these PO<sub>4</sub> adsorption data (Hiemstra and Zhao, 2016). In this approach, a previously described set of relationships (Hiemstra et al., 2019; Mendez and Hiemstra, 2020a) was iteratively used to calculate consistently the particle size-dependent molar mass ( $M_{\text{nano}}$ ) and density ( $\rho_{\text{nano}}$ ), as well as the size-dependent capacitances  $C_{1,2}$  for the inner and outer Stern layer (Hiemstra and Zhao, 2016).

## 2.2. Adsorption experiments

Stock solutions of 0.79 mM and 1.27 mM PMG were prepared in 0.01 M NaNO $_3$ , using glyphosate-isopropylamine provided by Bayer. Analysis of the stock solutions by liquid chromatography-tandem mass spectroscopy (LC-MS/MS) revealed no other compounds in measurable amounts. In addition, solutions of 10 mM NaH $_2$ PO $_4$ , 10 mM HNO $_3$ , 10 mM NaOH, and 10 mM NaNO $_3$  were prepared.

For the monocomponent PMG adsorption experiments, pH envelope experiments were performed for systems with 8 different total PMG concentrations. In a 15 mL tube, the required volume of 0.79 mM PMG stock was combined with 0.5 mL of the ferrihydrite suspension, and pH was adjusted by adding appropriate volumes of 10 mM NaOH or 10 mM HNO $_3$ , determined in a pre-experiment to ensure a suitable pH range and distribution of the 10 datapoints within that pH range. The samples were adjusted to 10 mL total volume using 10 mM NaNO $_3$  solution.

For the competition experiments, we used two total  $PO_4$  levels of 0.05 mM and 0.1 mM  $PO_4$ , selected to ensure PMG adsorption remained sufficiently high for accurate measurement. For each  $PO_4$  level, pH envelope experiments were performed for four total PMG concentrations by combining 1.27 mM PMG stock, 10 mM  $PO_4$ , and predetermined amounts of either 10 mM  $HNO_3$  or 10 mM NaOH with 0.5 mL of the ferrihydrite suspension, making up the final volume of 10 mL with 10 mM  $NaNO_3$ .

In all batch adsorption experiments, specific care was taken to avoid contamination with atmospheric  $\mathrm{CO}_2$ . The tubes were shaken for 24 h to reach a pseudo-equilibrium, after which they were centrifuged for 20 min at 3500 g. No replicates were included, as the collection of data at different concentration and pH conditions is favored for surface complexation modeling.

For both the monocomponent and the competition experiment, 5 mL of the supernatant was taken and acidified to 0.14 M HNO $_3$  for measuring total P with inductively coupled plasma-mass spectroscopy (ICP-MS). For the monocomponent PMG systems, this total P corresponds to the PMG in solution. For the competition experiments, PMG in solution was determined using LC-MS/MS, as described below. The concentration of PO $_4$  in the equilibrium solution could not be measured directly (Guo et al., 2025), and was calculated by subtracting the PMG-P concentration from the total P (ICP-MS) in the solution. In addition to P, Fe was measured with ICP-MS to assess the centrifugation efficacy. The pH was measured in the remaining 5 mL of the suspension.

PMG does not degrade in the presence of ferrihydrite (Li and Jaisi, 2019), and this was confirmed by the absence of transformation products detected in the LC-MS/MS measurements of the supernatant.

## 2.3. LC-MS/MS methodology

PMG in the supernatants of the PO<sub>4</sub> competition experiments was measured using a Shimadzu LC coupled with QTRAP 6500+ MS (Sciex). An anionic polar pesticide - hydrophilic interaction liquid chromatography (APP-HILIC) column was used (5  $\mu m,~2.1\times100$  mm, Waters). Water and acetonitrile were used as the mobile phase, both containing 0.9 % formic acid, starting at 10 % water with a linear increase to 85 % water in 4 min, which was subsequently held for 11 min. The flow rate was constant at 0.4 mL min $^{-1}$  throughout, and the column was kept at 35  $^{\circ}$ C. The injection volume was 10  $\mu L$ .

The mass spectrometer was operated in negative ionization mode using an electrospray ionization (ESI) interface, with a source

temperature of 550 °C and an ion spray voltage of -4 kV. Samples were diluted between 1 and 500 times to be measurable within the linear range of the calibration series of  $<0.1~\mu M$ . Measurement of the stock PMG solution showed that no other compounds were present in observable amounts.

#### 2.4. CD-MUSIC modeling

The surface characteristics of ferrihydrite have been described by the multisite ion complexation (MUSIC) model before (Hiemstra and Zhao, 2016), providing the surface sites and corresponding site densities. This model, based on the mineralogical bulk (Michel et al., 2010) and surface structure (Hiemstra, 2013), defines singly ( $\equiv$ FeOH<sup>-0.5</sup>), doubly (≡Fe<sub>2</sub>OH<sup>0</sup>), and triply (≡Fe<sub>3</sub>O<sup>-0.5</sup>) coordinated surface sites, with only the singly coordinated groups being able to engage in ligand exchange reactions. The model furthermore distinguishes between singly coordinated groups that can form mononuclear bidentate (edge-sharing) surface complexes (=FeOH(a)-0.5) and surface groups that can form binuclear bidentate (double-corner) surface complexes (=FeOH(b)<sup>-0.5</sup>), while both types of surface groups can form monodentate surface complexes. The corresponding site densities and surface reactions are provided in Table S1. In our modeling, the extended Stern model option was used to describe the compact part of the electrical double layer (Hiemstra and Van Riemsdijk, 2006).

Recently, X-ray absorption near edge structure (XANES) measurements (Li et al., 2023) confirm the formation of PMG innersphere complexes via the phosphonate group. In our modeling, we will distinguish series of bidentate and monodentate binding modes with differences in the protonation states of the -NH and -PO $_3$  group. The corresponding formation reactions are:

$$\equiv \text{FeOH(a,b)}^{-0.5} + \text{PMG}^{3-}(\text{aq}) + \text{H}^{+}(\text{aq}) \leftrightarrow \\ \equiv \text{FePMG}^{-2.5}(\text{a,b}) + \text{H}_2\text{O}\left(l\right) \tag{1}$$

$$\equiv\! FeOH(a,b)^{-0.5} + PMG^{3-}(aq) + 2H^{+}(aq) \leftrightarrow \equiv\! FePMGH^{-1.5}(a,b) + H_2O\left(l\right) \tag{2}$$

$$\equiv$$
 FeOH(a,b)<sup>-0.5</sup> +PMG<sup>3-</sup>(aq)+3H<sup>+</sup>(aq)  $\leftrightarrow$   $\equiv$  FePMGH<sub>2</sub><sup>-0.5</sup>(a,b)+H<sub>2</sub>O(l)
(3)

$$2 \equiv FeOH(b)^{-0.5} + PMG^{3-}(aq) + 2H^{+}(aq) \leftrightarrow \equiv Fe_{2}PMG^{-2}(b) + 2H_{2}O(l)$$
(4)

$$2 \equiv \text{FeOH(b)}^{-0.5} + \text{PMG}^{3-}(\text{aq}) + 3 \,\text{H}^{+}(\text{aq}) \leftrightarrow \equiv \text{Fe}_{2} \text{PMGH}^{-1}(\text{b}) + 2 \,\text{H}_{2} \text{O} \,(l)$$
(5)

$$2 \equiv FeOH(a)^{-0.5} + PMG^{3-}(aq) + 2~H^{+}(aq) \leftrightarrow \\ \equiv FePMG^{-2}(a) + 2~H_{2}O~(l) \eqno(6)$$

$$2 \equiv FeOH(a)^{-0.5} + PMG^{3-}(aq) + 3H^{+}(aq) \leftrightarrow \equiv FePMGH^{-1}(a) + 2H_{2}O(l) \tag{7}$$

where PMG<sup>3-</sup> (aq) is the fully deprotonated PMG compound in solution. The surface complexes formed by the reactions are displayed in Figure S1, and the surface complexes formed by the above reactions Eqs. (1)–(7) will be referred to as M, MH, MH<sub>2</sub>, and B, BH, Edge-B, and Edge-BH, respectively.

The solution speciation and surface complexation reactions for PO<sub>4</sub> are from Hiemstra and Zhao (2016) (Tables S1 and S2), and the solution speciation reactions of PMG are from Geysels et al. (2025b) (Table S2).

## 2.5. MO/DFT geometry optimization and charge distribution

The geometries of hydrated clusters of PMG and  $Fe_2(OH)_6(OH_2)_4$  forming monodentate and binuclear bidentate complexes have been optimized previously with MO/DFT (Geysels et al., 2025b), but expanded here for the mononuclear bidentate (edge) complexes. The  $6-31+G^{**}$  basis set and various functionals, i.e., B3LYP, EDF2,  $\omega$ B97X-D, and  $\omega$ B97X-V, were used.

The optimized geometries were used to derive the CD of the -PO<sub>3</sub> group by using the relative P-O bond lengths of the various complexes in the Brown bond valence approach (Brown and Altermatt, 1985). The resulting surface charge attribution was corrected for the dipole orientation of interfacial water (Hiemstra and Van Riemsdijk, 2006) to obtain the charge attribution coefficients  $\Delta z_0$ .

In the modeling, the charge attribution of adsorbed PMG to the outer Stern plane ( $\Delta z_2$ ) is expected to be primarily determined by the common non-protonated carboxylate group. For this charge attribution, we used a common value for all complexes, which was fitted as a free parameter. The charge attribution to the inner Stern plane ( $\Delta z_1$ ) follows the charge balance equation  $\Delta z_1 = \Delta z_{tot} - \Delta z_0 - \Delta z_2$  (Hiemstra and Van Riemsdijk, 2006) in which  $\Delta z_{tot}$  is the total added charge to the surface of the complex, equaling the sum of the charge of the reactants PMG<sup>3-</sup> and H<sup>+</sup> in Eqs. (1)–(7).

#### 2.6. Software and parameter optimization

The surface complexation model was implemented in ECOSAT v4.9 (Keizer and Van Riemsdijk, 1998) combined with FIT v2.581 (Kinniburgh, 1993) for parameter optimization. The affinity parameters of the surface complexes were fitted to the adsorption data, minimizing the difference between the calculated and measured percentage of PMG adsorption.

# 3. Results & discussion

# 3.1. PMG adsorption to ferrihydrite

The adsorption of PMG to ferrihydrite, displayed on a scale of percentage adsorbed, the absolute PMG surface loading ( $\Gamma$ ), and the logarithm of the solution concentration are shown in Fig. 1. The adsorption of PMG to ferrihydrite (point of zero charge = 8.1) shows a strong pH dependency, decreasing to nearly zero at pH > 9.5. The PMG surface loading shows a close to linear decrease with the increase of pH for total PMG that does not reach a nearly complete adsorption at low pH. This pH-dependency contrasts with the PMG sorption on goethite, where the increase in PMG surface loading diminishes with decreasing pH (Geysels et al., 2025b). A similar difference in the pH dependency is found for phosphate (Hiemstra and Zhao, 2016), which has been attributed to an enhanced protonation of the adsorbed PO<sub>4</sub> species.

Measured Fe concentrations in the supernatant were lower than 0.5 % of the total Fe. For 14 data points, the potential PMG loading on this remaining Fe contributed >1 % of the measured PMG. These points are removed from Fig. 1a.

# 3.2. PMG adsorption to ferrihydrite in competition with PO<sub>4</sub>

The results of the competitive adsorption experiments are shown in Figs. 2 and 3. At low pH, due to the high adsorption, 11 data points for dissolved PMG in Figs. 2a and 2b were below the limit of detection (LOD). The corresponding adsorption is given in Figs. 2c and 2d The LC-MS/MS methodology has an analytical variability of  $\sim$ 5 %, leading to several points in the high pH range with low PMG adsorption to be

B. Geysels et al. Water Research 288 (2026) 124634

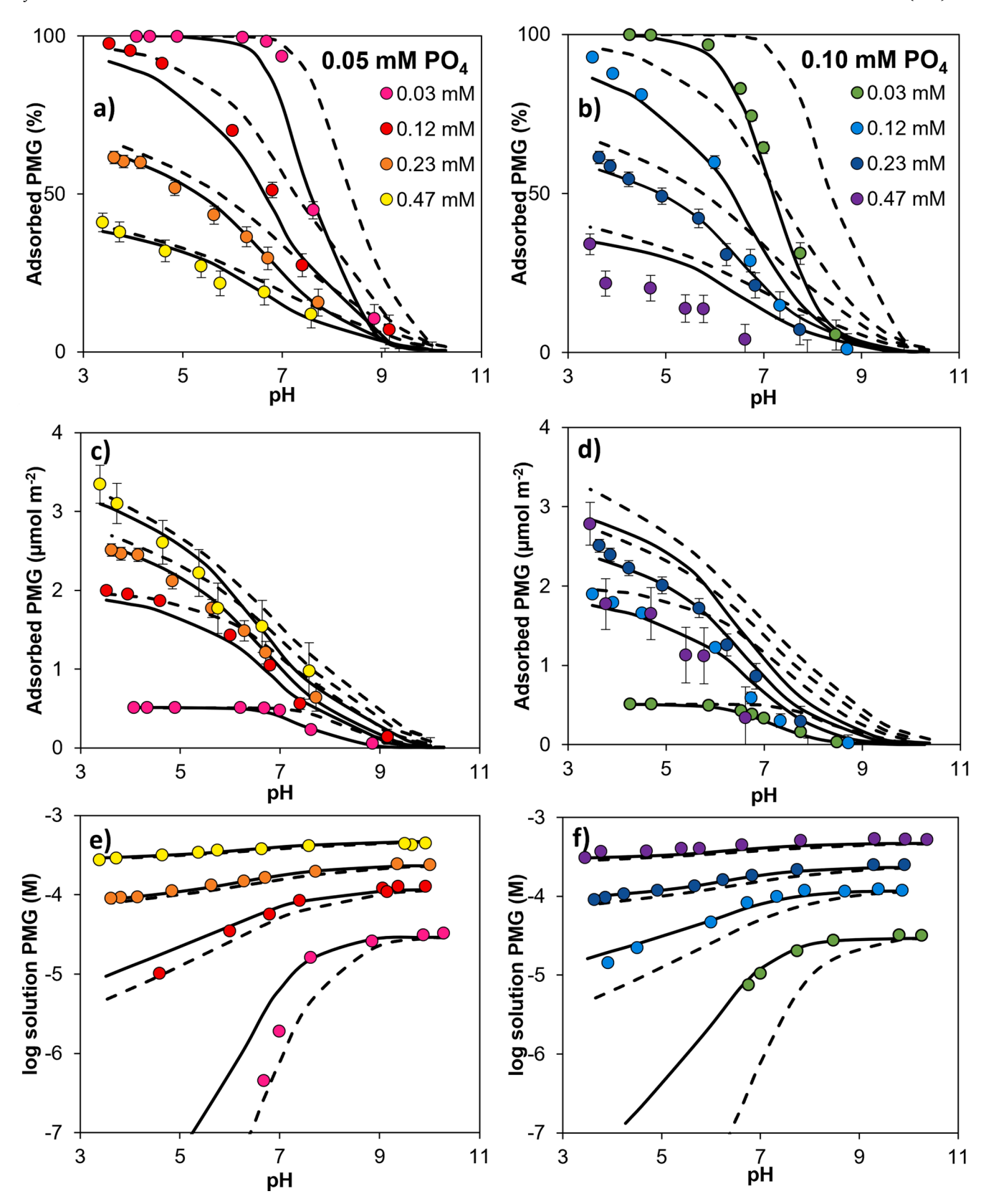


Fig. 2. Percentage adsorbed PMG (a,b), PMG surface loading (c,d), and corresponding logarithm of the equilibrium concentration in solution (e,f) as a function of pH in the competitive systems with 101 mg  $^{-1}$  ferrihydrite (569 m<sup>2</sup> g<sup>-1</sup>) in a background of 0.01 M NaNO<sub>3</sub> at two total PO<sub>4</sub> levels (0.05 mM and 0.1 mM). Solid lines represent model predictions using the parameters derived in this study (Table 1). For reference, the dashed lines represent the model calculations for the systems without PO<sub>4</sub>. Data points below LOD are not shown in (e) and (f). Error bars are calculated assuming an uncertainty of 5 % on the measured PMG solution concentration (absent error bars indicate the uncertainty is lower than the dot size of the symbols).

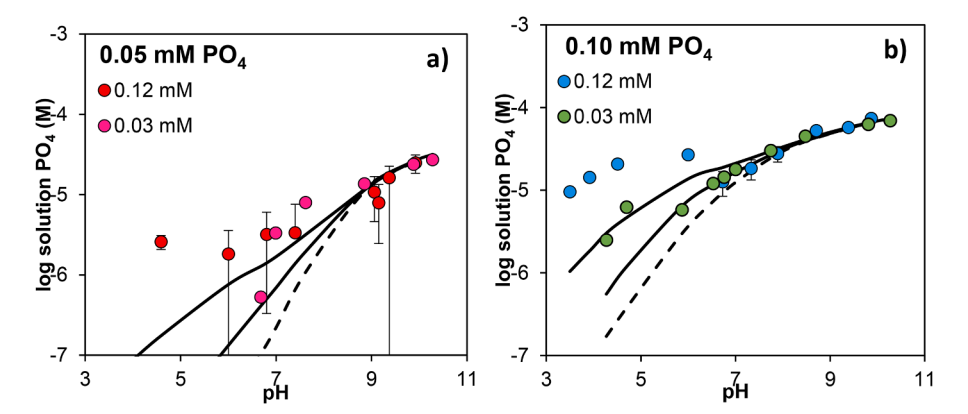


Fig. 3. Logarithm of the solution concentration of PO<sub>4</sub> measured in the competitive PMG-PO<sub>4</sub> systems of Fig. 2 containing 0.03 mM and 0.12 mM PMG in the presence of 0.05 mM (a) or 0.10 mM PO<sub>4</sub> (b), respectively. Solid lines represent the model predictions using the parameters derived for the monocomponent systems (Table 1). For reference, the dashed lines represent the model calculations for the systems without PMG. The effect of PMG on the PO<sub>4</sub> concentration is significantly smaller than that of PO<sub>4</sub> on the PMG adsorption, illustrating the stronger competition of PO<sub>4</sub> to PMG compared to vice-versa. Data points below LOD are not shown. Error bars are calculated assuming an uncertainty of 5 % on the measured PMG solution concentration (absent error bars indicate the uncertainty is lower than the dot size of the symbols).

measured as negative adsorption. These are consequently not shown in Fig. 2. Unremoved Fe in the supernatant did not contribute significantly to the solution P for the remaining data points.

Increasing PMG levels, logically, increase adsorbed PMG concentrations (Figs. 2c and d), a trend that deviates from the series with the highest PMG and  $PO_4$  concentration (Fig. 2d, 0.47 mM purple circles). In addition, 5 datapoints in this series show negative adsorption (Fig. 2b). This deviation is likely due to experimental error. As model parameters obtained by fitting were not affected by the inclusion of this series, the data was not excluded for the final model parameterization.

The data for the dissolved  $PO_4$  in the competition systems are given in Fig. 3. In part of the competition experiments, low amounts of dissolved  $PO_4$  cannot be quantified as these values follow experimentally from the difference between total P (ICP-MS) and P-PMG (LC-MS/MS), where the latter cannot be determined better than 5 %. Consequently, low concentrations of  $PO_4$  are overshadowed by relatively large values for dissolved PMG. The data in Figs. 3a and 3b are solely from the two experiments with the lowest PMG concentrations.

PMG concentrations in surface- and pore waters are typically  $\sim\!10^{-6}$  –  $10^{-7}$  in or near intensive agricultural areas (Mencaroni et al., 2023; Peruzzo et al., 2008). This range is included in the lower end of our experiments. Due to the selected PO<sub>4</sub> levels, the PO<sub>4</sub> concentration range in our experiments is significantly lower than in environmental systems. However, the impact of PO<sub>4</sub> at these levels is significant and measurable, and the mechanistic nature of the developed surface complexation model (see Final CD modeling) ensures it is applicable to conditions outside of the data used for calibration.

# 3.3. Initial CD modeling

In general, the pH dependency of the adsorption of charged species strongly depends on the location of the charge in the interface, particularly the charge attributed to the surface ( $\Delta z_0$ ). In addition, the protonation of the reactive ligands of the surface species controls the pH dependency. The concentration dependency and electrostatic competition of the adsorption is strongly regulated by the net charge outside the surface, particularly the charge in the 1-plane ( $\Delta z_1$ ). Only an appropriate combination of charge attribution allows a simultaneous description of both phenomena using a physically realistic set of surface species.

In our approach, parameter estimation for PMG was performed using  $\Delta z_0$  values derived from the geometries optimized with MO/DFT. The charge distribution outside the surface can be found by fitting the model to our experimental data, assuming a common value for  $\Delta z_2$  determined

by the ligand distribution of the -COO group (Geysels et al., 2025b). The value of  $\Delta z_1$  has multiple contributions, i.e., from the -PO<sub>3</sub> group as well as the protonation of the -NH and/or -PO<sub>3</sub> group, and its value follows from the charge balance as described in Materials and Methods.

In an initial attempt, we parameterized the CD model solely using the monocomponent adsorption data (Fig. 1), with the logK for each surface species and a common  $\Delta z_2$  as freely variable parameters. It provided a good fit, suggesting the surface complexes MH, MH<sub>2</sub>, B, and BH (Table S3), similar to those for goethite, without the need to consider the formation by edge-sharing complexes. These obtained parameters were applied to predict the competitive adsorption data, with PO<sub>4</sub> adsorption parameters from Hiemstra and Zhao (2016). However, this prediction is unsatisfactory (Figure S2), and PMG sorption in competition with PO<sub>4</sub> was underpredicted. This result demands another strategy to parameterize the model.

For PMG in the monocomponent systems (Fig. 1), the value fitted for  $\Delta z_2$  ( $-0.46 \pm 0.20$ , Table S3) is less negative than found for goethite (-0.74) (Geysels et al., 2025b). A less negative  $\Delta z_2$  value leads to more negative charge in the 1-plane, i.e., lower  $\Delta z_1$  values. The underprediction of PMG sorption in the competitive systems implies that glyphosate experiences a too strong electrostatic repulsion from adsorbed PO<sub>4</sub> ions, where the 1-plane is most important for electrostatic competition. Therefore, the common  $\Delta z_2$  for PMG must be more negative than suggested by the initial approach, as this would lead to less negative  $\Delta z_1$  values and, consequently, less electrostatic repulsion between PO<sub>4</sub> and PMG.

# 3.4. Final CD modeling

As the  $PO_4$  competition could not be sufficiently well predicted with the model parameterized solely using the monocomponent data, we included the PMG-PO<sub>4</sub> competition data. This revealed a surface speciation of B, BH, and MH<sub>2</sub> (Table 1). As shown with the model lines in Figs. 1 and 2, an excellent description was achieved for both data sets (with the exception of the deviating 0.47 mM glyphosate level at 0.10 mM PO<sub>4</sub>, purple series).

## 3.5. PMG surface speciation

The PMG surface speciation of ferrihydrite as a function of pH and at two different PMG levels was calculated with the parameters in Table 1. The results given in Fig. 4 illustrate a strong dominance of the bidentate surface complexes. This is particularly true for systems with low surface loading (Figs. 4c and 4d). Some doubly protonated monodentate

Table 1
Fitted logK values ( $\pm$  standard error) and CD coefficients for the PMG surface complexation of ferrihydrite using both the percentage adsorbed PMG from the monocomponent systems (Fig. 1a) and competitive systems (Figs. 2a and 2b). (RMSE = 4.68,  $r^2$  = 0.98).

Complex	Name	Reaction	$\Delta z_0^*$	$\Delta {z_1}^\#$	$\Delta z_2$	$\Delta z_{\mathrm{tot}}$	log K
≡Fe <sub>2</sub> PMG(b)	В	Eq. (4)	0.69	$-0.71~(\pm 0.04)$	$-0.98~(\pm 0.04)$	-1	24.32 (±0.11)
$\equiv$ Fe <sub>2</sub> PMGH(b)	BH	Eq. (5)	0.75	$0.23~(\pm 0.04)$	$-0.98~(\pm 0.04)$	0	$32.17~(\pm 0.05)$
$\equiv$ FePMGH <sub>2</sub> (a,b)	$MH_2$	Eq. (3)	0.41	$0.57~(\pm 0.04)$	$-0.98~(\pm 0.04)$	0	28.94 ( $\pm 0.21$ )

<sup>\*</sup> Calculated from MO/DFT geometry optimization.

<sup>&</sup>lt;sup>#</sup> Calculated from the charge balance  $\Delta z_1 = \Delta z_{\text{tot}} - \Delta z_0 - \Delta z_2$ .

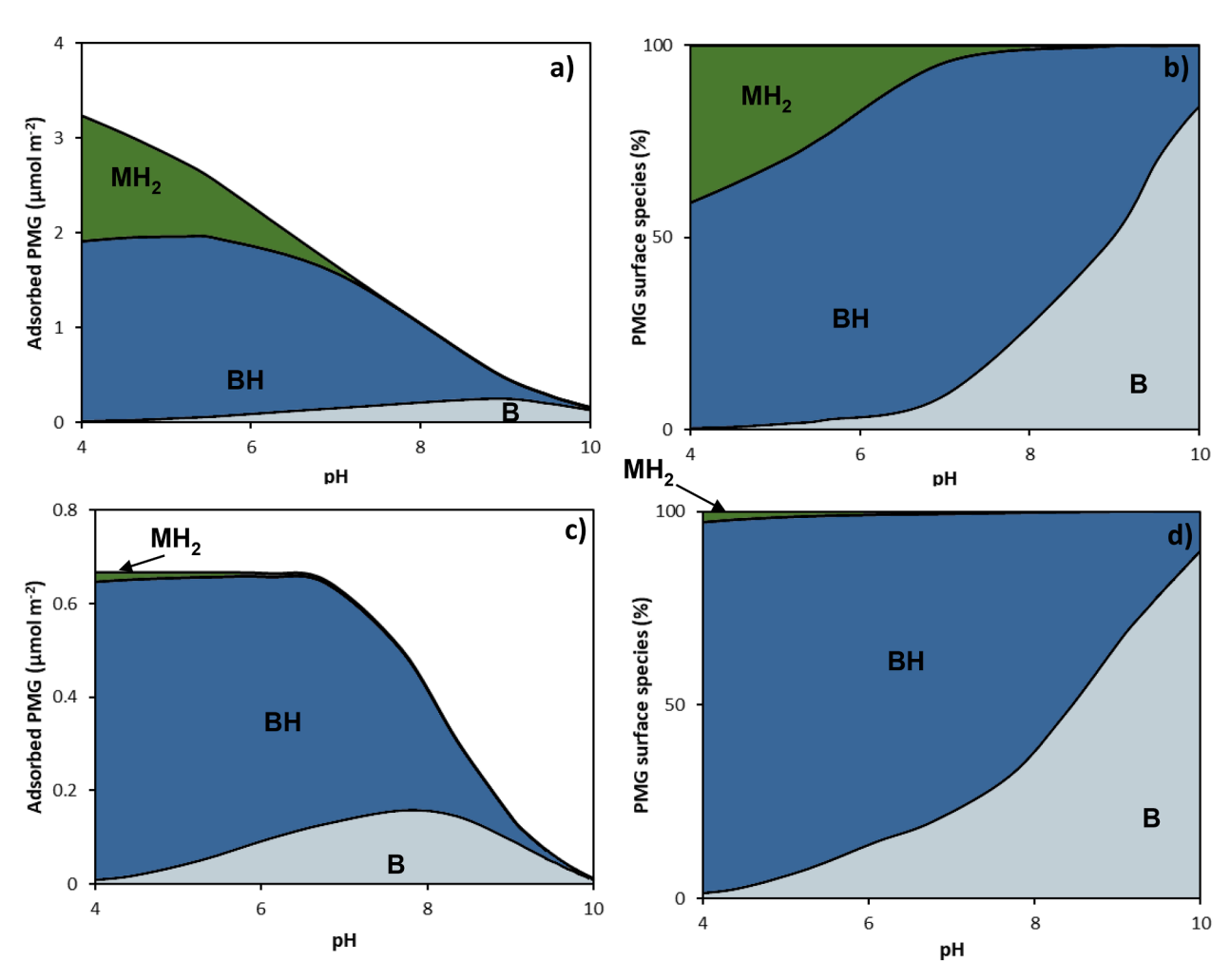


Fig. 4. Surface speciation and corresponding relative contribution of the surface species for PMG adsorbed to in 96 mg  $^{-1}$  ferrihydrite (618 m<sup>2</sup> g<sup>-1</sup>) systems with 0.01 M NaNO<sub>3</sub> as a background, calculated using the parameters of Table 1, for a total PMG concentration of 0.63 mM (a, b) or 0.04 mM (c, d).

complex formation (MH<sub>2</sub>) is found at low pH and high loading. At these conditions, the bidentate surface complexes account for up to  $\sim$ 2  $\mu$ mol m<sup>-2</sup> or occupy  $\sim$  2.4 sites nm<sup>-2</sup>, close to full saturation of the double corner sites (site density of  $\equiv$ FeOH(b) = 2.8 nm<sup>-2</sup>).

This speciation contrasts with the PMG surface speciation on goethite, where although bidentate binding is also dominant, monodentate binding modes are present throughout the pH and concentration range (Geysels et al., 2025b). It suggests that bidentate binding modes are favored on ferrihydrite and that these complexes outcompete monodentate modes, leading to the presence of some  $MH_2$  only at low pH and only in systems with a high loading. As these conditions create negative electrostatic potential in the 1- and 2-planes, protonation of MH to  $MH_2$  is promoted.

The domination of bidentate species is likely due to the enthalpic energy release of creating an additional Fe-O-P bond, which apparently exceeds the entropic energy cost of forming a double-corner complex.

Since the B and MH complexes are equivalent in proton coadsorption, one can interpret their formation as a theoretical M complex which adsorbs an additional proton. Here, we can speculate that the free energy release of forming a bidentate, by adsorption of the proton to the surface and releasing a water molecule, is higher than the energy release from protonation of the amino group of the M species. In other words, the energy release from the formation of the bidentate bridge will exceed the difference in proton affinities of the neighboring ≡FeOH group and the amino group of a M complex. While the proton affinity of the latter is unknown, as the species is not detected for either goethite or ferrihydrite, the proton affinity of the amino group for glyphosate in solution is ~10.8, while for a bidentate surface complex on goethite, the same proton affinity is  $\sim$ 8.2 (Geysels et al., 2025b) as the negative charge of PMG is partly neutralized by the Fe-O-P binding; the proton affinity of the amino group for a monodentate complex will likely be in between these two values. On the other hand, the proton affinity of a

≡FeOH group of goethite is reported as ~7.3 (Zhang et al., 2021), while for ferrihydrite, this value is ~8.0 (Hiemstra, 2013). This indicates that the protonation, and subsequent ligand exchange and water release, is more favorable for ferrihydrite than for goethite, which could explain the even stronger dominance of PMG bidentate binding modes for the former

In addition to the chemical affinity of the formation reaction, electrostatics also affect the speciation. Monodentate and bidentate complexes have significantly different CD coefficients for plane 0 and 1, which will affect the adsorption of the species and in turn change the electrostatic potential of the planes. Assessing the impact is complicated, as the potential of the individual planes affect each other, and furthermore affect the adsorption of other ions (e.g. protons), which further modify the electrostatic potential of one or more planes. The overall effect of these differences in CD coefficients might have the effect of favoring bidentate complexes over monodentate complexes in general, and specifically at high pH.

## 3.6. Proton affinity of the surface complexes

Fig. 4 illustrates the importance of the protonation of the bidentate PMG species. The protonation of the surface complexes is essential for describing the adsorption of PMG to ferrihydrite. The protonation reaction  $B + H^+$  (aq)  $\leftrightarrow$  BH with  $log K_H = 7.9 \pm 0.2$  concerns the protonation of the amino group of PMG. This value is comparable to the value found by modeling for goethite ( $log K_H = 8.2 \pm 0.5$ ) (Geysels et al., 2025b).

The protonation of the monodentate surface complexes (MH+ $H^+$ (aq) ↔ MH<sub>2</sub>) refers to the -PO<sub>3</sub> group. For goethite, we found a proton affinity constant of  $log K_H = 5.3$  for this reaction. Using this value to calculate a theoretical binding affinity of the MH species for ferrihydrite of logK=25.6. When this complex is added to our CD model, a considerable contribution of this species is predicted. This indicates that for ferrihydrite, the proton affinity of the monodentate surface complex must be higher and, correspondingly, the binding affinity MH must be lower, otherwise, the contribution of the singly protonated MH surface complex would be found with modeling. This higher logK<sub>H</sub> value will transform MH into MH2, making the MH species minor or absent, and unresolvable in the modeling. A higher proton affinity for -PO  $_3$  bound to ferrihydrite fits in the general trend of relatively high proton affinities for oxyanion surface complexes bound to ferrihydrite compared to the same complexes for goethite (Hiemstra and Zhao, 2016). By contrast, the logK<sub>H</sub> for the bidentate complex is not different for ferrihydrite and goethite, but this concerns the protonation of the amino group of PMG situated further away on the molecular chain, where it does not directly interact with the metal (hydr)oxide surface.

## 3.7. Spectroscopy

Spectroscopic studies of glyphosate adsorption to ferrihydrite are scarce and only provide information for a limited pH and concentration range (Li et al., 2023; Pereira et al., 2019). In addition, ferrihydrite properties are notably dependent on the preparation protocol, storage and post-synthesis treatment. Here, we note that Pereira et al. (2019) lyophilized the ferrihydrite after synthesis, and Li et al. (2023) stored their ferrihydrite suspension for an unreported amount of time, after which the suspension was deposited on a ZnSe crystal and air-dried for the FTIR measurements. These treatments promote crystal growth, leading to a lower SSA, and can affect the primary surface charge and point-of-zero-charge of the mineral (Mendez and Hiemstra, 2020a), which in turn affects the speciation of adsorbed ions. This yields an exact comparison of our reported surface speciation to the literature reported FTIR spectra impossible. Nevertheless, some qualitative insights can be obtained.

Pereira et al. (2019) reported FTIR spectra for lyophilized ferrihydrite with adsorbed PMG samples at a likely surface loading of 0.5–2

 $\mu$ mol m<sup>-2</sup> for pH 2–6. Near  $\sim$ 1400 cm<sup>-1</sup>, the invariant vibrational band can be attributed to the symmetric -COO stretching that indicates the absence of considerable protonation of the carboxylate group (Geysels et al., 2025b). A reasonable consistent vibrational band is observed at  $\sim$ 1600 cm<sup>-1</sup>. This band can be assigned to asymmetric -COO stretching but is influenced by the protonation of the amino group (Sheals et al., 2002). The spectra of Pereira et al. (2019) show no indication of a deprotonating amino group in the pH range 2–6, which is in line with our modeling (Figs. 4a and 4b).

Li et al. (2023) reported on the phosphonate range (900–1200 cm<sup>-1</sup>) of the PMG spectra at pH 5 and 9 in 0.01 M NaCl for an equilibrium concentration of 50 mg l<sup>-1</sup>, equivalent to a surface loading of  $\sim$ 3 and  $\sim$ 0.3 µmol m<sup>-2</sup> respectively, as calculated for our fresh ferrihydrite. The spectra at pH 5 and 9 are remarkably similar, showing major peaks at  $\sim$ 980 cm<sup>-1</sup>,  $\sim$ 1055 cm<sup>-1</sup>,  $\sim$ 1125 cm<sup>-1</sup>. Minor peaks are observed at  $\sim$ 950 cm<sup>-1</sup>,  $\sim$ 1020 cm<sup>-1</sup>,  $\sim$ 1090 cm<sup>-1</sup>, and  $\sim$ 1150 cm<sup>-1</sup>. These are assigned to two components, of which one is dominant ( $\sim$ 75 %). The authors speculated that the corresponding dominant surface species was monodentate, however, our surface speciation (Figs. 4a and 4b) shows the dominant species to be a bidentate, while the minor surface species could be a monodentate or a bidentate in a different protonation state.

Relative to the major component observed by Li et al. (2023), the frequencies of the minor one are shifted to higher wavenumbers by ~30 cm<sup>-1</sup>. According to our MO/DFT frequency calculations, the wavelengths for BH are typically 20-30 cm<sup>-1</sup> higher than the equivalent wavelengths for the B complexes, while the wavelengths of both MH and  $MH_2$  are a further ~30 cm<sup>-1</sup> higher (Figure S3). This supports our CD-MUSIC modeling result that bidentate surface complexes are the major species on ferrihydrite. Providing our reported surface speciation (Fig. 4) the FTIR spectrum at pH 9 would suggest the major bands can be assigned to B and the minor bands to BH, while the spectrum at pH 5 rather suggests the major bands could be assigned to BH and the minor bands to MH2. We therefore hypothesize that the synthesis and post-treatment of the ferrihydrite of Li et al. (2023) yielded a mineral with sufficiently distinct charging properties from our ferrihydrite, which significantly affects the ratio of B and BH complexes. Another possibility is that the crystallization of the ferrihydrite of Li et al. (2023) during storage and drying yielded a mineral with goethite-like properties, which exhibits a rather constant ratio of a dominant BH and minor MH complex throughout the pH range of 5-9 (Geysels et al., 2025b).

For ferrihydrite, the dominant species has three major well-developed -PO $_3$  bands, of which the middle one is at  $\sim 1055 \pm 10$  cm  $^1$ . This band is also found for glyphosate bound to goethite (Barja and Dos Santos Afonso, 2005; Orcelli et al., 2018; Sheals et al., 2002; Yan and Jing, 2018), but there it is less intense and obscured by other contributions (MH and B) on either side. Our MO/DFT calculations suggest three peaks for the BH surface complex. These peaks are related to the stretching of the -P=O double bond, and the asymmetric  $v_{as}(P-OFe)$  and symmetric v(P-O stretching), which can be positioned after scaling at  $\sim 1130$  cm  $^{-1}$ ,  $\sim 1060$  cm  $^{-1}$ , and  $\sim 980$  cm  $^{-1}$ , respectively (Figure S3). The MH species similarly has three peaks, but these are shifted to higher wavenumbers ( $\Delta \sim 30$  cm  $^{-1}$ ).

## 3.8. Interfacial charge distribution of PMG complexes

As discussed above, the charge distribution of PMG over the 1- and 2-plane depends on the chosen fitting strategy. A more negative  $\Delta z_2$  value is found when the PMG-PO $_4$  competition data are included. By intentionally adding different levels of PO $_4$ , the electrostatic double layer potentials can be varied, allowing a better resolution of the CD coefficients. Without PO $_4$ , the variation of the Stern layer potentials is solely due to the variation in the PMG surface loading.

Our final  $\Delta z_2$  value of -0.98 (Table 1) suggests a full contribution of the carboxylate charge to the outer Stern plane, which can be understood from the dominance of the bidentate complexes having a structure perpendicularly bound to the surface (Figure S1). The -COO group can

B. Geysels et al. Water Research 288 (2026) 124634

effectively enter the second Stern layer. Monodentate complexes can bind in a more oblique conformation (Figure S1) and the interfacial ligand distribution of the -COO group may differ, contributing less charge to the 2-plane. In that case, the average value of  $\Delta z_2$  will depend on the mono- to bidentate surface complex ratio. This could explain the lower value of  $\Delta z_2$  found for goethite (-0.74) compared to ferrihydrite (-0.98), as the former oxide has relatively more monodentate complex formation. Unfortunately, differentiating between  $\Delta z_2$  values for monodentate and bidentate binding modes cannot resolve this due to an excess of free parameters.

#### 4. Conclusion

In this study, we developed and parameterized a surface complexation model for glyphosate binding to the nano-oxide ferrihydrite particles. In the parameterization of the model using only monocomponent glyphosate adsorption data, we encountered the limitations of this method for complex compounds with multiple ionizable functional groups, coinciding with increasing numbers of freely fitted parameters. However, this limitation was overcome by including competitive adsorption data. In our study, phosphate was included as a competitor and shown to be crucial in controlling the sorption of glyphosate in environmental systems, and likely leading to incomplete removal of glyphosate in conventional wastewater treatment. In addition, the oxyanion also acted to intentionally change the electrostatic double layer potential profile of the ferrihydrite systems, allowing an improved parameterization of the charge distribution coefficients of the surface complexes, thus distinguishing between chemical and electrostatic contributions to the adsorption.

We found that glyphosate primarily binds as a bidentate complex of which the amino group can protonate ( $\log K_{\rm H}=7.9$ ). Monodentate binding of glyphosate is only prominent at high surface loadings and low pH, when surface sites for bidentate sorption become scarce. In these conditions, glyphosate binds via a monodentate surface complex with protonated amino and phosphonate group.

The surface speciation of glyphosate on ferrihydrite shows differences to its speciation to goethite, extending our understanding of the distinct properties of nano-sized ferrihydrite. Similar to the earlier observations, for ferrihydrite, we found enhanced protonation of the ligands directly interacting with the surface. For glyphosate, this results in the absence of a non-protonated monodentate species at the ferrihydrite interface. In contrast, the ligands that do not directly interact with the surface show similar protonation affinities for ferrihydrite and goethite.

Our parametrized CD model provides a mechanistic and quantitative understanding of the surface speciation and interfacial electrostatics of glyphosate bound to ferrihydrite. The surface speciation was supported by literature FTIR spectra, which were analyzed using MO/DFT calculated theoretical spectra of the surface species. Our model is directly usable for environmental applications and provides a generic description of the sorption and fate of glyphosate in soils and sediments, using ferrihydrite as a proxy.

## CRediT authorship contribution statement

Bram Geysels: Writing – original draft, Visualization, Validation, Software, Methodology, Investigation, Formal analysis, Data curation, Conceptualization. Tjisse Hiemstra: Writing – review & editing, Supervision, Software, Investigation, Formal analysis. Arnoldus W.P. Vermeer: Writing – review & editing, Supervision, Conceptualization. Jan E. Groenenberg: Writing – review & editing, Supervision, Methodology, Conceptualization.

## Declaration of competing interest

The authors declare the following financial interests/personal relationships which may be considered as potential competing interests: Bram Geysels reports financial support was provided by INVITE GmbH. If there are other authors, they declare that they have no known competing financial interests or personal relationships that could have appeared to influence the work reported in this paper.

## Acknowledgments

This research was funded by Invite GmbH. Joost Memelink and Gerco den Hertog are gratefully acknowledged for the arrangements and execution of the HPLC-MS measurements, and Peter Nobels for performing the ICP measurements.

## Supplementary materials

Supplementary material associated with this article can be found, in the online version, at doi:10.1016/j.watres.2025.124634.

## Data availability

The data will be made available at doi:10.4121/46fbbfbb-d8b6-413c-90bc-93c2b38513ae

#### References

- Arroyave, J.M., Waiman, C.C., Zanini, G.P., Avena, M.J., 2016. Effect of humic acid on the adsorption/desorption behavior of glyphosate on goethite. Isotherms kinet. Chemosph. 145, 34–41. https://doi.org/10.1016/j.chemosphere.2015.11.082.
- Arroyave, J.M., Waiman, C.C., Zanini, G.P., Tan, W., Avena, M.J., 2017. Desorption rate of glyphosate from goethite as affected by different entering ligands: hints on the desorption mechanism. Env. Chem. 14, 288. https://doi.org/10.1071/EN17004.
- Barja, B.C., Dos Santos Afonso, M., 2005. Aminomethylphosphonic acid and glyphosate adsorption onto goethite: a comparative study. Env. Sci. Technol. 39, 585–592. https://doi.org/10.1021/es035055q.
- Borggaard, O.K., Gimsing, A.L., 2008. Fate of glyphosate in soil and the possibility of leaching to ground and surface waters: a review. Pest. Manage Sci. 64, 441–456. https://doi.org/10.1002/ps.1512.
- Botta, F., Lavison, G., Couturier, G., Alliot, F., Moreau-Guigon, E., Fauchon, N., Guery, B., Chevreuil, M., Blanchoud, H., 2009. Transfer of glyphosate and its degradate AMPA to surface waters through urban sewerage systems. Chemosphere 77, 133–139. https://doi.org/10.1016/j.chemosphere.2009.05.008.
- Brown, I.D., Altermatt, D., 1985. Bond-valence parameters obtained from a systematic analysis of the inorganic crystal structure database. Acta Crystallogr. B 41, 244–247. https://doi.org/10.1107/S0108768185002063.
- Carretta, L., Masin, R., Zanin, G., 2022. Review of studies analysing glyphosate and aminomethylphosphonic acid (AMPA) occurrence in groundwater. Env. Rev. 30, 88–109. https://doi.org/10.1139/er-2020-0106.
- Day, G.M., Hart, B.T., McKelvie, I.D., Beckett, R., 1997. Influence of natural organic matter on the sorption of biocides onto goethite. II. Glyphosate. Env. Technol. 18, 781–794. https://doi.org/10.1080/09593331808616597.
- De Gerónimo, E., Aparicio, V.C., 2022. Changes in soil pH and addition of inorganic phosphate affect glyphosate adsorption in agricultural soil. Eur. J. Soil. Sci. 73, e13188. https://doi.org/10.1111/ejss.13188.
- De Jonge, H., De Jonge, L.W., Jacobsen, O.H., Yamaguchi, T., Moldrup, P., 2001. Glyphosate sorption in soils of different ph and phosphorus content. Soil. Sci. 166, 230–238. https://doi.org/10.1097/00010694-200104000-00002.
- Dideriksen, K., Stipp, S.L.S., 2003. The adsorption of glyphosate and phosphate to goethite: a molecular-scale atomic force microscopy study. Geochim. Cosmochim. Acta 67, 3313–3327. https://doi.org/10.1016/S0016-7037(02)01369-8.
- Geysels, B., Groenenberg, J.E., Hiemstra, T., Apreza Arrieta, H.S., Vermeer, A.W.P., Comans, R.N.J., 2025a. Steric hindrance of glyphosate adsorption to metal (Hydr) oxides: a novel model approach for organic matter-mineral interactions. Env. Sci. Technol. https://doi.org/10.1021/acs.est.5c04207.
- Geysels, B., Hiemstra, T., Groenenberg, J.E., Comans, R.N.J., 2025b. Glyphosate binding and speciation at the water-goethite interface: a surface complexation model consistent with IR spectroscopy and MO/DFT. Water. Res. 273, 123031. https://doi. org/10.1016/j.watres.2024.123031.
- Gimsing, A.L., Borggaard, O.K., 2007. Phosphate and glyphosate adsorption by hematite and ferrihydrite and comparison with other variable-charge minerals. Clays Clay Min. 55, 108–114. https://doi.org/10.1346/CCMN.2007.0550109.
- Guo, H., Barnard, A.S., 2013. Naturally occurring iron oxide nanoparticles: morphology, surface chemistry and environmental stability. J. Mater. Chem. A 1, 27–42. https:// doi.org/10.1039/C2TA00523A.
- Guo, R., Röhnelt, A.M., Martin, P.R., Haderlein, S.B., 2025. Limitations of the molybdenum blue method for phosphate quantification in the presence of organophosphonates. Anal. Bioanal. Chem. 417, 3103–3111. https://doi.org/ 10.1007/s00216-025-05850-y.
- Hanke, I., Wittmer, I., Bischofberger, S., Stamm, C., Singer, H., 2010. Relevance of urban glyphosate use for surface water quality. Chemosphere 81, 422–429. https://doi. org/10.1016/j.chemosphere.2010.06.067.

- Hébert, M., Fugère, V., Gonzalez, A., 2019. The overlooked impact of rising glyphosate use on phosphorus loading in agricultural watersheds. Front. Ecol. Env. 17, 48–56. https://doi.org/10.1002/fee.1985.
- Hiemstra, T., 2018. Ferrihydrite interaction with silicate and competing oxyanions: geometry and Hydrogen bonding of surface species. Geochim. Cosmochim. Acta 238, 453–476. https://doi.org/10.1016/j.gca.2018.07.017.
- Hiemstra, T., 2013. Surface and mineral structure of ferrihydrite. Geochim. Cosmochim. Acta 105, 316–325. https://doi.org/10.1016/j.gca.2012.12.002.
- Hiemstra, T., Mendez, J.C., Li, J., 2019. Evolution of the reactive surface area of ferrihydrite: time, pH, and temperature dependency of growth by Ostwald ripening. Env. Sci. Nano. 6, 820–833. https://doi.org/10.1039/C8EN01198B.
- Hiemstra, T., Van Riemsdijk, W.H., 2006. On the relationship between charge distribution, surface hydration, and the structure of the interface of metal hydroxides. J. Colloid. Interface Sci. 301, 1–18. https://doi.org/10.1016/j. icis.2006.05.008.
- Hiemstra, T., Zhao, W., 2016. Reactivity of ferrihydrite and ferritin in relation to surface structure, size, and nanoparticle formation studied for phosphate and arsenate. Env. Sci. Nano 3, 1265–1279. https://doi.org/10.1039/C6EN00061D.
- Jambor, J.L., Dutrizac, J.E., 1998. Occurrence and constitution of natural and synthetic ferrihydrite, a widespread iron oxyhydroxide. Chem. Rev. 98, 2549–2586. https:// doi.org/10.1021/cr970105t.
- Jonsson, C.M., Persson, P., Sjöberg, S., Loring, J.S., 2008. Adsorption of glyphosate on goethite (α-FeOOH): surface complexation modeling combining spectroscopic and adsorption data. Env. Sci. Technol. 42, 2464–2469. https://doi.org/10.1021/ cs/270966b
- Keizer, M.G., Van Riemsdijk, W.H., 1998. ECOSATFITmanual.pdf.
- Kinniburgh, D.G., 1993. Technical Report WD/93/23 FIT User Guide
- Laitinen, P., Siimes, K., Rämö, S., Jauhiainen, L., Eronen, L., Oinonen, S., Hartikainen, H., 2008. Effects of soil phosphorus status on environmental risk assessment of glyphosate and glufosinate-ammonium. J. Env. Qual. 37, 830–838. https://doi.org/ 10.2134/jeq2007.0256.
- Li, H., Jaisi, D.P., 2019. Competition of sorption and degradation reactions during glyphosate degradation by ferrihydrite/δ-manganese oxide composites. ACS. Earth. Space Chem. 3, 1362–1370. https://doi.org/10.1021/acsearthspacechem.9b00127.
- Li, X., Yang, P., Zhao, W., Guo, F., Jaisi, D.P., Mi, S., Ma, H., Lin, B., Feng, X., Tan, W., Wang, X., 2023. Adsorption mechanisms of glyphosate on ferrihydrite: effects of al substitution and aggregation state. Env. Sci. Technol. 57, 14384–14395. https://doi.org/10.1021/acs.est.3c04727.
- Likus, M., Komorowska-Kaufman, M., Pruss, A., Zych, Ł., Bajda, T., 2021. Iron-based water treatment residuals: phase, physicochemical characterization, and textural properties. Materials 14, 3938. https://doi.org/10.3390/ma14143938.
- Livi, K.J.T., Villalobos, M., Ramasse, Q., Brydson, R., Salazar-Rivera, H.S., 2023. Surface site density of synthetic goethites and its relationship to atomic surface roughness and crystal size. Langmuir. 39, 556–562. https://doi.org/10.1021/acs. langmuir.2c02818.
- Mencaroni, M., Longo, M., Cardinali, A., Lazzaro, B., Zanin, G., Dal Ferro, N., Morari, F., 2023. Glyphosate and AMPA dynamics during the transition towards conservation agriculture: drivers under shallow groundwater conditions. Soil. Tillage Res. 229, 105659. https://doi.org/10.1016/j.still.2023.105659.
  Mendez, J.C., Hiemstra, T., 2020a. Surface area of ferrihydrite consistently related to
- Mendez, J.C., Hiemstra, T., 2020a. Surface area of ferrihydrite consistently related to primary surface charge, ion pair formation, and specific ion adsorption. Chem. Geol. 532, 119304. https://doi.org/10.1016/j.chemgeo.2019.119304.
- Mendez, J.C., Hiemstra, T., 2020b. High and low affinity sites of ferrihydrite for metal ion adsorption: data and modeling of the alkaline-earth ions Be, Mg, Ca, Sr, Ba, and Ra. Geochim. Cosmochim. Acta 286, 289–305. https://doi.org/10.1016/j.gca.2020.07.032.
- Mendez, J.C., Hiemstra, T., Koopmans, G.F., 2020. Assessing the reactive surface area of soils and the association of soil organic carbon with natural oxide nanoparticles using ferrihydrite as proxy. Env. Sci. Technol. 54, 11990–12000. https://doi.org/10.1021/acs.est.0c02163
- Mendez, J.C., Van Eynde, E., Hiemstra, T., Comans, R.N.J., 2022. Surface reactivity of the natural metal (hydr)oxides in weathered tropical soils. Geoderma 406, 115517. https://doi.org/10.1016/j.geoderma.2021.115517.
- Michel, F.M., Barrón, V., Torrent, J., Morales, M.P., Serna, C.J., Boily, J.-F., Liu, Q., Ambrosini, A., Cismasu, A.C., Brown, G.E., 2010. Ordered ferrimagnetic form of ferrihydrite reveals links among structure, composition, and magnetism. Proc. Natl. Acad. Sci. 107, 2787–2792. https://doi.org/10.1073/pnas.0910170107.
- Munira, S., Farenhorst, A., Flaten, D., Grant, C., 2016. Phosphate fertilizer impacts on glyphosate sorption by soil. Chemosphere 153, 471–477. https://doi.org/10.1016/j. chemosphere.2016.03.028.
- Ololade, I.A., Oladoja, N.A., Oloye, F.F., Alomaja, F., Akerele, D.D., Iwaye, J., Aikpokpodion, P., 2014. Sorption of glyphosate on soil components: the roles of metal oxides and organic materials. soil sediment contam. Int. J. 23, 571–585. https://doi.org/10.1080/15320383.2014.846900.

- Orcelli, T., Di Mauro, E., Urbano, A., Valezi, D.F., Da Costa, A.C.S., Zaia, C.T.B.V., Zaia, D.A.M., 2018. Study of interaction between glyphosate and goethite using several methodologies: an environmental perspective. Water. Air. Soil. Pollut. 229, 150. https://doi.org/10.1007/s11270-018-3806-1.
- Pereira, R.C., Anizelli, P.R., Di Mauro, E., Valezi, D.F., Da Costa, A.C.S., Zaia, C.T.B.V., Zaia, D.A.M., 2019. The effect of pH and ionic strength on the adsorption of glyphosate onto ferrihydrite. Geochem. Trans. 20, 3. https://doi.org/10.1186/s12932-019-0063-1.
- Peruzzo, P.J., Porta, A.A., Ronco, A.E., 2008. Levels of glyphosate in surface waters, sediments and soils associated with direct sowing soybean cultivation in north pampasic region of Argentina. Env. Pollut. 156, 61–66. https://doi.org/10.1016/j.envpol.2008.01.015.
- Poiger, T., Keller, M., Buerge, I.J., Balmer, M.E., 2020. Behavior of glyphosate in wastewater treatment plants. CHIMIA 74, 156. https://doi.org/10.2533/ chimia.2020.156.
- Qu, Z., Wu, Y., Zhu, S., Yu, Y., Huo, M., Zhang, L., Yang, J., Bian, D., Wang, Y., 2019. Green synthesis of magnetic adsorbent using groundwater treatment sludge for tetracycline adsorption. Engineering 5, 880–887. https://doi.org/10.1016/j. eng.2019.06.001.
- Schwientek, M., Rügner, H., Haderlein, S.B., Schulz, W., Wimmer, B., Engelbart, L., Bieger, S., Huhn, C., 2024. Glyphosate contamination in European rivers not from herbicide application? Water. Res. 263, 122140. https://doi.org/10.1016/j. waters 2024 122140
- Sheals, J., Granström, M., Sjöberg, S., Persson, P., 2003. Coadsorption of Cu(II) and glyphosate at the water–goethite (α-FeOOH) interface: molecular structures from FTIR and EXAFS measurements. J. Colloid. Interface Sci. 262, 38–47. https://doi. org/10.1016/S0021-9797(03)00207-8.
- Sheals, J., Sjöberg, S., Persson, P., 2002. Adsorption of glyphosate on goethite: molecular characterization of surface complexes. Env. Sci. Technol. 36, 3090–3095. https:// doi.org/10.1021/es010295w.
- Sprankle, P., Meggitt, W.F., Penner, D., 1975. Adsorption, mobility, and microbial degradation of glyphosate in the soil. Weed. Sci. 23, 229–234. https://doi.org/ 10.1017/S0043174500052929.
- Sun, M., Li, H., Jaisi, D.P., 2019. Degradation of glyphosate and bioavailability of phosphorus derived from glyphosate in a soil-water system. Water. Res. 163, 114840. https://doi.org/10.1016/j.watres.2019.07.007.
- Van Eynde, E., Hiemstra, T., Comans, R.N.J., 2022. Interaction of Zn with ferrihydrite and its cooperative binding in the presence of PO4. Geochim. Cosmochim. Acta 320, 223–237. https://doi.org/10.1016/j.gca.2022.01.010.
- Van Eynde, E., Mendez, J.C., Hiemstra, T., Comans, R.N.J., 2020. Boron adsorption to ferrihydrite with implications for surface speciation in soils: experiments and modeling. ACS. Earth. Space Chem. 4, 1269–1280. https://doi.org/10.1021/ acsearthspacechem.0c00078.
- Venditti, S., Kiesch, A., Hansen, J., 2023. Fate of glyphosate and its metabolite AminoMethylPhosponic acid (AMPA) from point source through wastewater sludge and advanced treatment. Chemosphere 340, 139843. https://doi.org/10.1016/j. chemosphere.2023.139843.
- Waiman, C.V., Arroyave, J.M., Chen, H., Tan, W., Avena, M.J., Zanini, G.P., 2016. The simultaneous presence of glyphosate and phosphate at the goethite surface as seen by XPS, ATR-FTIR and competitive adsorption isotherms. Colloids Surf. Physicochem. Eng. Asp 498, 121–127. https://doi.org/10.1016/j. colsurfa.2016.03.049.
- Waiman, C.V., Avena, M.J., Garrido, M., Fernández Band, B., Zanini, G.P., 2012. A simple and rapid spectrophotometric method to quantify the herbicide glyphosate in aqueous media. Application to adsorption isotherms on soils and goethite. Geoderma 170. 154–158. https://doi.org/10.1016/j.geoderma.2011.11.027.
- Geoderma 170, 154–158. https://doi.org/10.1016/j.geoderma.2011.11.027. Waiman, C.V., Avena, M.J., Regazzoni, A.E., Zanini, G.P., 2013. A real time in situ ATR-FTIR spectroscopic study of glyphosate desorption from goethite as induced by phosphate adsorption: effect of surface coverage. J. Colloid. Interface Sci. 394, 485–489. https://doi.org/10.1016/j.jcis.2012.12.063.
- Yan, W., Jing, C., 2018. Molecular insights into glyphosate adsorption to goethite gained from ATR-FTIR, two-dimensional correlation spectroscopy, and DFT study. Env. Sci. Technol. 52, 1946–1953. https://doi.org/10.1021/acs.est.7b05643.
- Zhang, B., Wang, L., Li, Y., 2019. Fractionation and identification of iron-phosphorus compounds in sewage sludge. Chemosphere 223, 250–256. https://doi.org/ 10.1016/j.chemosphere.2019.02.052.
- Zhang, Q., Li, Y., Kroeze, C., Xu, W., Gai, L., Vitsas, M., Ma, L., Zhang, F., Strokal, M., 2024. A global assessment of glyphosate and AMPA inputs into rivers: over half of the pollutants are from corn and soybean production. Water. Res. 261, 121986. https://doi.org/10.1016/j.watres.2024.121986.
- Zhang, Y., Liu, X., Cheng, J., Lu, X., 2021. Interfacial structures and acidity constants of goethite from first-principles molecular dynamics simulations. Am. Miner. 106, 1736–1743. https://doi.org/10.2138/am-2021-7835.